Nanoscale

In situ Characterization of Kinetics and Mass Transport of PbSe Nanowire Growth via LS and VLS Mechanisms

Journal:	*Nanoscale*
Manuscript ID	NR-COM-02-2019-001200
Article Type:	Communication
Date Submitted by the Author:	07-Feb-2019

Complete List of Authors:	Song, Miao; Pacific Northwest National Laboratory, Physical and Computational Sciences Directorate Lee, Jaewoon; Pacific Northwest National Laboratory, Physical and Computational Sciences Directorate Wang, Bin; Pacific Northwest National Laboratory, Physical and Computational Sciences Directorate; Xi'an Jiaotong University, School of Science, MOE Key Laboratory for Non-equilibrium Synthesis and Modulation of Condensed Matter, State Key Laboratory for Mechanical Behavior of Materials Legg, Benjamin A; Pacific Northwest National Laboratory, Physical and Computational Sciences Directorate Hu, Shenyang; Pacific Northwest National Laboratory, Energy and Environment Directorate Chun, Jaehun; Pacific Northwest National Laboratory, Experimental & Computational Engineering Li, Dongsheng; Pacific Northwest National Laboratory,

Nanoscale

COMMUNICATION

In situ Characterization of Kinetics and Mass Transport of PbSe Nanowire Growth via LS and VLS Mechanisms

Received 00th January 20xx,
Accepted 00th January 20xx

DOI: 10.1039/x0xx00000x

www.rsc.org/

Miao Song,[a] Jaewon Lee,[a] Bin Wang,[a, b] Benjamin A. Legg,[a] Shenyang Hu,[c] Jaehun Chun,[a] Dongsheng Li*[a]

We grew binary PbSe nanowires in an *in situ* gas-heating cell in a transmission electron microscope and elucidated species dependent mass transport pathways and key correlation among supersaturation, nucleation, and growth kinetics, thereby enabling morphological and compositional control of nanowires with tailored properties.

Vapor-liquid-solid (VLS) growth is a commonly observed nanowire growth mechanism. In this mechanism, vapor precursors are concentrated by a catalytic liquid droplet, allowing a solid crystalline nanowire to subsequently grow at the liquid-solid interface ($I_{L/S}$)[1-4]. Nanowire VLS growth is generally believed to proceed by a mono-nuclear layer-by-layer process, where just one nucleation event occurs per added growth layer (as the timescale for growing a layer is much shorter than the timescale for nucleating a new layer, which occurs at the VLS triple junction)[5, 6]. Although investigations into growing nanowire structures with controlled diameter[7], morphology[8, 9], composition[10], growth direction[11], and heterojunctions[6, 12] have shown great success, the complete growth mechanism is not yet fully understood. Recent advances in *in situ* transmission electron microscope (TEM) techniques have allowed atomic scale studies of the steady state VLS growth process, providing new insights on the heterogeneous interface structure[12] and interface kinetics[13, 14]. However, because of the difficulties in capturing the fleeting early stages of nanowire formation, little is known regarding the earliest stages of growth, which are critical for the eventual nanowire size[1], growth direction[11], and phase[15]. In particular, questions remain as to whether growth proceeds by mono-nuclear or poly-nuclear process at the $I_{L/S}$ during the early stages. Thus, investigations into the early evolution of the interface are a critical step for achieving a comprehensive understanding of nanowire growth.

Moreover, few *in situ* studies have focused on compound nanowires[14, 16], which are challenging to study, due to the need to carefully control complicated reaction parameters such as temperature gradient[13, 14] and precursor purity[16, 17]. The growth mechanism of compound nanowires is also more complicated than that of a single elemental nanowire due to the complex mass transport pathways that can occur, associated with the presence of multiple growth precursors. For example, during Al_2O_3 nanowire VLS growth, the Al precursors are supplied from the vapor phase directly, while oxygen is provided by transient sacrificial dissolution of the top rim areas of nanowires[18]. Another study on the binary Gallium Phosphide (GaP) system showed that when Ga and P growth species were asymmetrically supplied at a low partial pressure ratio of precursors P/Ga (<100), the liquid catalyst surface absorbed Ga and acted as a reservoir for Ga while the P precursor was transported directly from gas phase and reacted with Ga on the catalyst surface[16]. Such mass-transport phenomena enable new controls over nanowire composition, with direct gas-phase transport making it possible to rapidly change precursor composition, and avoid the reservoir effects that inhibit precise control of elemental composition during growth of hetero-structure nanowires[2]. Therefore, understanding mass transport pathways during compound nanowire growth may enable the production of nanowires with complex hetero-structures, unique properties, and novel functionalities.

Here we studied a compound nanowire of lead selenide (PbSe). As a special class of IV-VI narrow-band-gap semiconductor[19] that exhibit excellent quantum confinement at the nanoscale[20], PbSe has been extensively investigated,

[a] *Physical and Computational Sciences Directorate, Pacific Northwest National Laboratory, Richland, WA 99352, USA. E-mail: Dongsheng.Li2@pnnl.gov*
[b] *School of Science, MOE Key Laboratory for Non-equilibrium Synthesis and Modulation of Condensed Matter, State Key Laboratory for Mechanical Behavior of Materials, Xi'an Jiaotong University, Xi'an, 710049, China*
[c] *Energy and Environment Directorate, Pacific Northwest National Laboratory, Richland, WA 99352, USA*

†Electronic Supplementary Information (ESI) available: [Experimental, morphological evolution of precursors during *in situ* heating, the evolution of the curved solid/liquid interface, *ex situ* EDS analysis after cooling to room temperature, surface tension induced lattice strain near the triple-phase interface, two nucleations in one droplet, supersaturated growth species at stage I, length measurement standard and growth mechanism during stage II, direct observation of PbSe wire growth by VLS mechanism, step-growth mechanism on top {200} surface, vapor species in TEM heating cell during heating, nucleation rate and layer growth rate, growth kinetics based on different growth models, width difference]. See DOI: 10.1039/x0xx00000x

including fundamental research[14, 21] and practical applications[22]. In this work, we explored the early stages of nanowire growth and investigated how the growth mechanisms and mass transport pathways of Pb and Se precursors changed during the course of crystal growth.

We used a gas-heating cell holder mounted in a TEM for the direct observation of the growth of the PbSe nanowire, which presented as a nanorod due to limited growth time and precursors (Fig. 1, Movie S1, see supporting information (SI)-1 for experimental details). PbSe and Bi metal powders (Fig. S1) were deposited on the heating chips of the gas cell, to serve as precursor and catalyst, respectively. To generate a supersaturated environment for PbSe nanorod growth[17, 18], the gas heating cell was heated up to 900°C for several minutes and then quickly cooled to 525°C under an environment of a mixed gas of 5% H_2 in N_2 at 4×10^3 Pa (See SI-1 for experimental details). At 900°C, the Bi catalyst formed amorphous liquid Bi droplets and the PbSe partially volatilized (Fig. S3). During cooling, PbSe nucleated and grew within the amorphous liquid droplet (Fig. 1a-f), where the crystal structure and amorphous phase were identified by HRTEM imaging (Fig. 1g) and fast Fourier transform (FFT, Fig. 1h and i). During the first 17 s, the crystal grew rapidly and the initially curved $I_{L/S}$ (Fig. 1a and 1g) evolved into a straight interface on the (200) plane (Fig. 1c). This straightening is believed to be driven by a reduction in surface energy, due to the high energy of the curved surface compared with the lowest surface energy of PbSe $\{200\}$[23]. During straightening, the growth plane advanced from the PbSe crystal toward the liquid droplet (Fig. 1j) indicating that the initial growth did not follow a regular VLS mechanism. Throughout this process, the PbSe crystal remained in the same orientation $[001]$ (Fig. S4), indicating the observed curvature was indeed caused by a curved interface rather than the projection of a tilted flat round interface (see also SI-3). The source of the initial interface curvature is unknown; it may reflect early-stage growth kinetics, potentially reflecting recent suggestions that diffusive transport can be faster through the bulk than near the droplet periphery[24]. After 17 s, the $I_{L/S}$ had become flat, but the rapid growth of PbSe continued in that direction for an additional 37 s. We defined the growth process during these initial ~54 s as stage I based on growth direction and rate (see the discussion regarding growth rate below). After ~54 s, the PbSe crystal started to grow into a nanorod along the $\langle100\rangle$ direction, which is reversed from the stage I growth direction (Fig. 1d-f, and k), while the liquid droplet and $I_{L/S}$ position remained nearly unchanged (Fig. 1k). This growth process was consistent with previously reported VLS growth and we defined it as stage II. EDS analysis (Fig. S5a) after heating confirmed that the liquid droplet and the nanorod (Fig. 1) were composed of Bi/Pb and Pb/Se, respectively.

In addition, due to the unbalanced surface tension (γ) of γ_{VL}, γ_{VS}, and γ_{LS} at the triple-phase junction (J_{TP}), lattice strain (ε) was observed in PbSe crystal with the ~4% expansion of $d_{(200)}$and ~3% shriking of $d_{(020)}$ (Fig. 2a, b, and d) at 0 s. The ε decreased to ~0 when the relative position (r/R, r is the radial distance from the center of the spherical cap (Fig. 1b) to the position where ε was measured and R is the radius of the spherical cap) moved from the J_{TP} (r/R= 1) to $r/R \leq 0.5$. After the $I_{L/S}$ became flat (17s), the ε_{xx} became 0 (Fig. 2d and f) indicating that γ_{VL} and γ_{VS} were roughly equal. This result is consistent with the values of γ_{VL} (0.35-0.45 J/m^2 [25]) and γ_{VS} (0.32-0.42 J/m^2 [23]) from literatures. ε_{YY} at r/R=0.95 was stabilized at ~0.04 after 17s due to the fixed direction of γ_{LS} (Fig. 2f). When the $I_{L/S}$ was curved, the x ($\gamma_{LS}cos\theta$) and y ($\gamma_{LS}sin\theta$) components of γ_{LS} resulted in the ε_{XX} and ε_{YY}(Fig. 2e) , respectively, because γ_{VL} and γ_{VS} cancelled out each other. Our experimental results showed that $-\varepsilon_{XX}/\varepsilon_{YY}$ and $\gamma_{LS}cos\theta/\gamma_{LS}sin\theta$ are well consistent (Fig. 2d), further demonstrating that ε_{XX} and ε_{YY} are mainly induced by the x and y components of γ_{LS} (see SI-4). However, the chemistry in liquid drop and at the interfaces may change with time due to the segregation and depletion of species at the interface. This affects γ, hence, ε. During growth stage II (see discussion below), nucleation occurs at the J_{TP}, at which lattice distortion usually increases the nucleation barrier, especially for epitaxial growth like PbSe. Therefore, it is needed to further study the effect of material process parameters on lattice strain at the J_{TP}, PbSe nucleation, and growth kinetics.

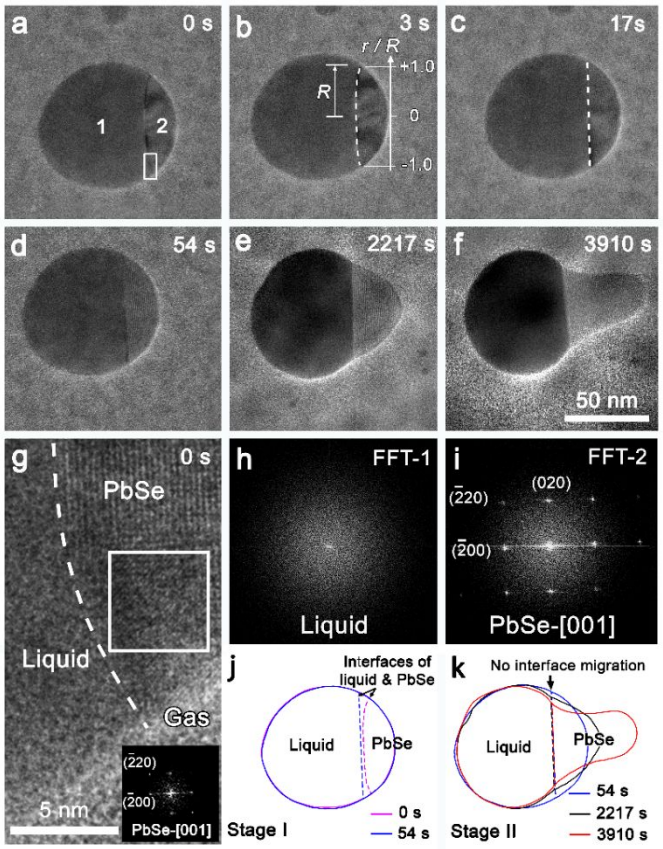

Fig. 1 *In situ* growth process of a PbSe nanorod at 525°C. (a-f) Sequential HRTEM images of PbSe nanorod during growth. The first image (0 s) was captured after cooling 2 min. $I_{L/S}$ is delineated by the white-dashed line. (g) Enlarged HRTEM images of white-boxed areas in (a). (h) and (i) FFT images of the liquid droplet and the PbSe crystal, respectively. (j) and (k) Outlines of liquid droplets (solid lines) and $I_{L/S}$ (dashed lines) during growth.

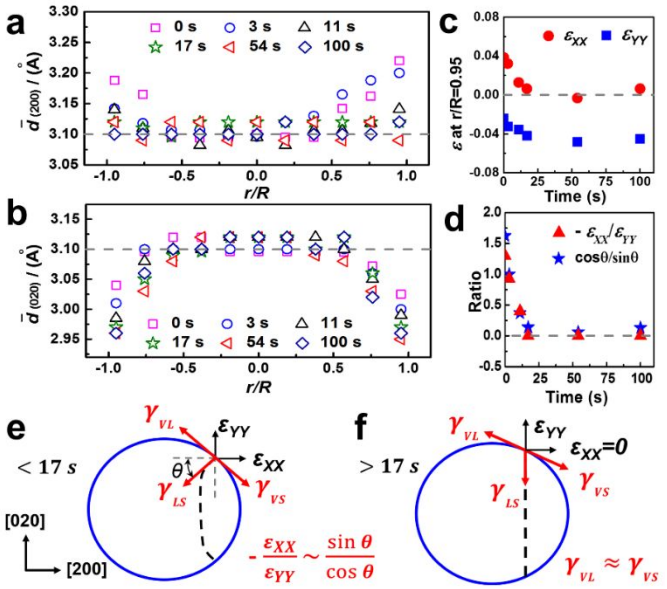

Fig. 2 Surface tension induced lattice strain. (a) and (b) d spacings of (200) and (020), respectively, at various time and r/R. (c) Plot of ε with time at the r/R=0.95. (d) Comparison of the ratios of $-\varepsilon_{XX}/\varepsilon_{YY}$ and $cos\theta/sin\theta$. Schematic illustration of γ and ε at J_{TP} for (e) < 17 s and (f) > 17 S.

HRTEM images (Fig. 3a) verified that the wire grew via a poly-nuclei growth process during stage I; *i.e.*, PbSe nucleated synchronously at multiple sites (islands) on the $I_{L/S}$ with numerous step edges available for growth (Fig. 3a). The islands had different heights of 4–8 layers of $\{200\}$ and were distributed across the $I_{L/S}$. PbSe grew fast on these step edges by direct deposition of highly supersaturated growth species (Fig. 3b-d). A second PbSe particle in the liquid droplet (Fig. S7, SI-6-7) indicated a high supersaturation of growth species[26] in the Bi liquid during the initial growth stage.

During stage II, $I_{L/S}$ remained straight and there were no islands or nucleation on $I_{L/S}$, for example, at 2563 s (Fig. 3e). A new step of two layers of (200) plane emerged at the top J_{TP} after a further 24 s of *in situ* heating at 525°C (Fig. 3f). No other nucleation or growth of PbSe was observed on the interface (Fig. S8e and j, SI-8), indicating that only one nucleus formed on J_{TP} during each layer's growth, corresponding to a mono-nuclear VLS growth process[6]. After layer nucleation, PbSe epitaxially and laterally grew across the (200) plane interface (Fig. 3h). This VLS mono-nuclear and fast lateral growth process were also verified by more *in situ* low magnification (LM) TEM experiments (SI 9-10). Therefore, stage II corresponds to a well-known VLS-controlled growth process[5, 6]; *i.e.*, the catalytic Bi liquid droplet absorbed precursors from the vapor phase, which crystallized at the $I_{L/S}$ leading to the growth of PbSe crystal along the $\langle 100 \rangle$ direction. However, the mass transport of the precursors during compound growth was more complex than that of a single element crystal, and limited knowledge[16, 18] was obtained in previous work. Here, we analyzed the precursor transport pathways by *in situ* composition analysis.

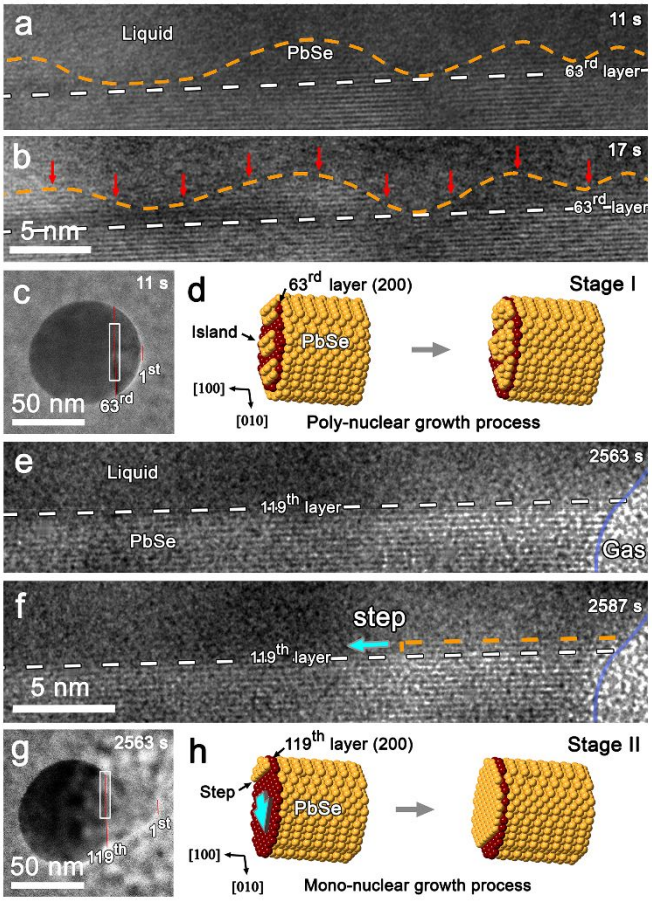

Fig. 3 Growth mechanisms of a PbSe nanorod. (a) and (b) HRTEM images of $I_{L/S}$ (white-boxed area in (c) with 90° rotation) showing island growth (poly-nuclear mechanism) at 525°C at 11 s and 17 s, respectively. (c) A TEM image of a liquid droplet at 11s. (d) A schematic illustration of the poly-nuclear growth mechanism of stage I. (e) and (f) HRTEM images of $I_{L/S}$ (white-boxed area in (g) with 90° rotation), showing VLS lateral growth (mono-nuclear mechanism) at 525°C at 2563 s and 2587 s, respectively. (g) A TEM image of wire growth at 2563 s. (h) A schematic illustration of the mono-nuclear lateral growth mechanism of stage II. The 63rd layer in (c) and the 119th layer in (g) were identified by lattice intensity profiles (SI-7). The red spheres in (d) and (h) denoted the atoms on the 63rd layer and the 119th layer of PbSe {200} atomic plane, respectively.

In situ EDS elemental mapping and composition analysis during the VLS growth process (stage II) at 525°C (Fig. 4) showed that the nanorod was composed of Pb and Se with an atomic ratio of ~1 (Fig. 4b), while analysis of multiple liquid droplets showed that they consisted of Bi and Pb, with Pb atomic ratios ranging from 0 to 85 at. % (Fig. 4c). The wide range of Pb concentrations found in the Bi liquid droplets is consistent with the full Bi-Pb liquid miscibility shown in the binary Bi-Pb phase diagram (Fig. S11b). No Se was detected in the liquid catalyst from *in situ* EDS analysis of numerous Bi catalysts (Fig. 4b-c and Fig. S5b). Unlike Pb, Se had limited solubility in Bi liquid (Fig. S11c) and was depleted after initial LS growth. Due to the presence of H_2 gas in the TEM cell, Se vapor is expected to react form H_2Se gas[27]. The theoretical equilibrium partial pressures of Se and PbSe at 525°C are 1.2×10^{-8} Pa and 1.6×10^{-7} Pa[28], respectively, which are significantly

lower than that of H_2Se (~ 200 Pa, calculated based on 5 vol. % H_2 in mixed carrier gas at a pressure of 4×10^3 Pa, SI-11). Therefore, Se precursors were supplied from a mixed-vapor phase of PbSe, Se, and H_2Se, with H_2Se dominating (SI-11). Based on the EDS results and phase diagram analysis, we conclude that Pb and Se were supplied separately from liquid and vapor phases, respectively, during the stage II growth. As the main Se precursor, H_2Se from the gas phase will diffuse into the liquid at the J_{TP} and react with Pb precursor in the liquid phase, inducing growth of the PbSe nanorod. The slow mass transport of Se precursor from vapor to liquid surface kinetically limited the PbSe nanorod growth, leading to a significantly slow wire growth rate (~0.36 nm/min, Fig. 5) during stage II. On the other hand, during stage I (Fig. 4d), the poly-nucleation and fast growth rate of ~3.3 nm/min indicate a high supersaturation in contrast to stage II. In addition, the PbSe crystal grew inside the Bi droplet indicating a direct deposition of precursors through bulk diffusion in Bi liquid onto the $I_{L/S}$ instead of VLS. Therefore, during stage I, both Pb and Se elements were present in the liquid catalyst droplet and served as growth species leading to a poly-nuclear LS growth process (Fig. 3).

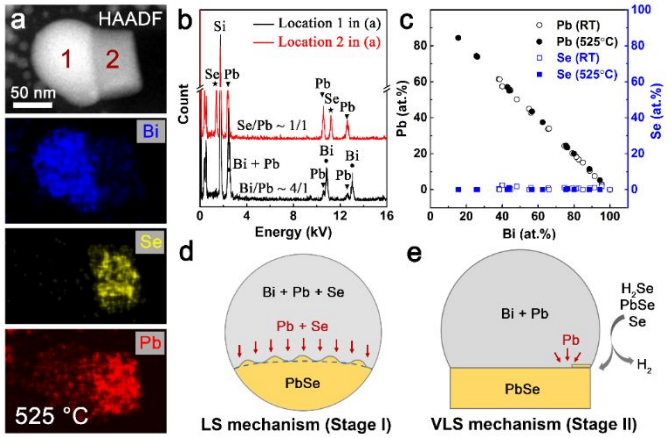

Fig. 4 *In situ* EDS composition analysis. (a) EDS mapping of a PbSe nanorod during the growth process at 525°C. (b) In situ EDS spectra of the droplet and nanorod (a). (c) Composition analysis of Pb and Se atomic percentages from numerous Bi liquid droplet at 525°C and room temperature (RT). (d) and (e) Schematic illustrations of two growth mechanisms and corresponding mass transport pathways.

Beside mass transport pathways, the significant difference of growth rates of stage I and II was also related to the supersaturation variation. Higher saturations during stage I will promote higher nucleation rates[29], Thus, the poly-nuclear growth process during stage I is an indication of higher saturation.

The different growth kinetics of stages I and II can be quantified using a generalized Avrami model[30]. The ratio of layer nucleation rate (I_n), to the lateral growth rate (v), is quantified by the parameter $\alpha = \pi I_n R^3/v$ (where R is the interface radius). Values of $\alpha \gg 1$ correspond to a poly-nuclear mechanism, while values of $\alpha \ll 1$, correspond to a mono-nuclear mechanism[30]. Based on the experimental growth kinetics during stage I, the estimated minimum α_{min} (~ 434) is much larger than 1 (SI-12), indicating a poly-nuclear process. During stage II, the estimated maximum α_{max} (~ 0.6) is less than 1 based on minimum v ($v = 1/t_I$, t_I is lateral growth time for each layer). In the calculation, t_I is estimated by experimental layer growth time, which includes nucleation time (t_N) and t_I (SI-12). Generally, the t_N is significantly longer than that of the t_I during VLS growth process[6]. Therefore, the real α is $\ll$ 1 (SI-12), and corresponds to a mono-nuclear process. The nucleation mechanism theory based on experimental growth kinetics was consistent with our *in situ* observation of nucleation. In addition, we estimated the rate of nanorod growth (V), *as a* function of h (the average high of nucleus), I_n and v. When $\alpha \gg 1$, $V = h(\pi v^2 I_n/3)^{1/3}$; when $\alpha \ll 1$, $V = h\pi R^2 I_n$[30]. The calculated V of stage I and stage II are 5.4 nm/min and 0.72 nm/min (SI-12), respectively, which were in the same order of magnitude as the measured $V$of ~3.3 nm/min and 0.36 nm/min (Fig. 5). The results of growth kinetics analysis are consistent with our *in situ* observation of poly- and mono-nuclear processes and grow rates during stage I and II.

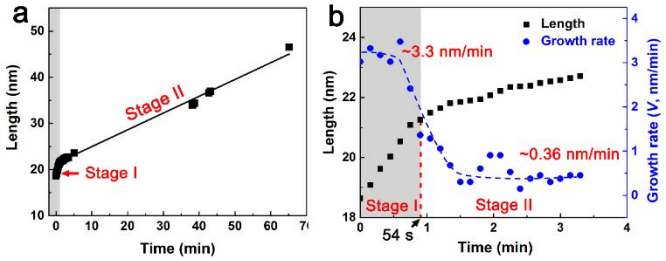

Fig. 5 Growth kinetics of the PbSe nanorod. (a) PbSe nanorod length along the $\langle 100 \rangle$ direction as a function of growth time during in situ heating at 525°C. (b) Plots of PbSe wire length vs. time and growth rate during initial 3.3 min showing significant growth rate change at ~ 54 s. (See SI-8 for length measurement method)

During growth stage II, we noticed that the diameter of the PbSe nanorod in our TEM gas cell (Fig. 1i) was thinner than that of the $I_{L/S}$. This was most likely due to PbSe evaporation, which was verified by *in situ* heating of the PbSe powder in TEM (Fig. S3c-f, see SI-13 for details), due to the limited amount of precursor in the vapor phase instead of atom migration and shape evolution. The significant wire width difference between the *in situ* HRTEM experiment (tens of nanometers) and *in situ* LM TEM experiments (nanometers to microns, Fig. S9-10 and 14) is associated with specific experimental conditions, *i.e.* the quantity of precursor powders supplied in experiments (see SI-14 for details).

In summary, our study revealed that PbSe nanowires may undergo an initial LS growth stage before later transitioning to the traditional VLS growth pathway. Changes in growth mechanism are related to supersaturation and mass transport of precursors. Higher supersaturation during the early LS stage led to faster nucleation of new crystal layers and produced a poly-nuclear growth mechanism, rather than the traditional mono-nuclear process. This highlights the strong correlation among supersaturation, mass transport pathways, and growth kinetics, all of which must be considered in order to quantitatively explain the nucleation and growth mechanisms and enable control over nanowire growth. Our findings

showed that variation in the solubility of growth species and chemical reaction with the vapor phase played a key role in controlling mass transport pathways, which will enable the possibility of controlling the composition, crystal size, and structure of nanowires that have unique properties.

Conflicts of interest

There are no conflicts to declare.

Acknowledgement

We thank Ben Mills and Matt Chipman from Gatan, Ronald Marx from DENSsolutions, and Ben Jacobs, Robert Monteverde, Kate Marusak, and Remy Berthier from Protochips for demonstrating in-situ gas heating holders and partial data collection. This research was supported by the U.S. Department of Energy (DOE), Office of Science, Office of Basic Energy Sciences (BES), Early Career Research program under Award #67037. Surface tension analysis was partially supported by the DOE-BES, Synthesis Science and Processing Program. The work was partially conducted in the William R. Wiley Environmental Molecular Sciences Laboratory (EMSL), a national scientific user facility sponsored by the DOE Office of Biological and Environmental Research and located at Pacific Northwest National Laboratory (PNNL). PNNL is a multiprogram national laboratory operated for the U.S. Department of Energy by Battelle under Contract No. DE-AC05-76RLO1830.

Notes and references

1. E. I. Givargizov, *J. Cryst. Growth*, 1975, **31**, 20-30.
2. M. R. Frances, *Rep. Prog. Phys.*, 2010, **73**, 114501.
3. Y. Aswani, M. Enrico, P. Martin, T. H. Annal, K. Ute and T. Wolfgang, *Angew. Chem.*, 2009, **48**, 6426-6430.
4. L. Geunhee, W. Y. Sung, Y. Jee-Eun, L. Donghun, K. Cheol-Joo and J. Moon-Ho, *Angew. Chem.*, 2009, **48**, 7366-7370.
5. C. Y. Wen, J. Tersoff, M. C. Reuter, E. A. Stach and F. M. Ross, *Phys. Rev. Lett.*, 2010, **105**, 195502.
6. C. Y. Wen, M. C. Reuter, J. Bruley, J. Tersoff, S. Kodambaka, E. A. Stach and F. M. Ross, *Science*, 2009, **326**, 1247-1250.
7. Y. Cui, L. J. Lauhon, M. S. Gudiksen, J. Wang and C. M. Lieber, *Appl. Phys. Lett.*, 2001, **78**, 2214-2216.
8. Y. Fang, Y. Jiang, M. J. Cherukara, F. Shi, K. Koehler, G. Freyermuth, D. Isheim, B. Narayanan, A. W. Nicholls, D. N. Seidman, S. K. R. S. Sankaranarayanan and B. Tian, *Nat. Commun.*, 2017, **8**, 2014.
9. J. B. Hannon, S. Kodambaka, F. M. Ross and R. M. Tromp, *Nature*, 2006, **440**, 69-71.
10. O. Moutanabbir, D. Isheim, H. Blumtritt, S. Senz, E. Pippel and D. N. Seidman, *Nature*, 2013, **496**, 78-82.
11. V. Schmidt, S. Senz and U. Gösele, *Nano Lett.*, 2005, **5**, 931-935.
12. F. Panciera, Y. C. Chou, M. C. Reuter, D. Zakharov, E. A. Stach, S. Hofmann and F. M. Ross, *Nat. Mater.*, 2015, **14**, 820-826.
13. J. Zhu, H. Peng, C. K. Chan, K. Jarausch, X. F. Zhang and Y. Cui, *Nano Lett.*, 2007, **7**, 1095-1099.
14. J. Zhu, H. Peng, A. F. Marshall, D. M. Barnett, W. D. Nix and Y. Cui, *Nat. Nanotechnol.*, 2008, **3**, 477-481.
15. S. Jia, S. Hu, H. Zheng, Y. Wei, S. Meng, H. Sheng, H. Liu, S. Zhou, D. Zhao and J. Wang, *Nano Lett.*, 2018, **18**, 4095-4099.
16. Y. C. Chou, K. Hillerich, J. Tersoff, M. C. Reuter, K. A. Dick and F. M. Ross, *Science*, 2014, **343**, 281-284.
17. K. Tateno, G. Zhang, H. Gotoh and T. Sogawa, *Nano Lett.*, 2012, **12**, 2888-2893.
18. S. H. Oh, M. F. Chisholm, Y. Kauffmann, W. D. Kaplan, W. Luo, M. Rühle and C. Scheu, *Science*, 2010, **330**, 489-493.
19. S. D. Mahanti, K. Hoang and S. Ahmad, *PHYSICA B*, 2007, **401-402**, 291-295.
20. D. V. Talapin and C. B. Murray, *Science*, 2005, **310**, 86-89.
21. M. J. Bierman, Y. K. A. Lau, A. V. Kvit, A. L. Schmitt and S. Jin, *Science*, 2008, **320**, 1060-1063.
22. S. J. Oh, N. E. Berry, J.-H. Choi, E. A. Gaulding, H. Lin, T. Paik, B. T. Diroll, S. Muramoto, C. B. Murray and C. R. Kagan, *Nano Lett.*, 2014, **14**, 1559-1566.
23. C. Fang, M. A. van Huis, D. Vanmaekelbergh and H. W. Zandbergen, *ACS Nano*, 2010, **4**, 211-218.
24. H. Wang, L. A. Zepeda-Ruiz, G. H. Gilmer and M. Upmanyu, *Nat Commun*, 2013, **4**, 1956.
25. R. Novakovic, E. Ricci, D. Giuranno and F. Gnecco, *Surface Science*, 2002, **515**, 377-389.
26. Y. Xia, P. Yang, Y. Sun, Y. Wu, B. Mayers, B. Gates, Y. Yin, F. Kim and H. Yan, *Adv. Mater.*, 2003, **15**, 353-389.
27. B. E. Langner, *Ullmann's Encyclopedia of Industrial Chemistry*, 2005, **32**, 343-355.
28. J. C. Lin, R. C. Sharma and Y. A. Chang, *J. Phase Equilib.*, 1996, **17**, 253-260.
29. S. Biswas, C. O'Regan, N. Petkov, M. A. Morris and J. D. Holmes, *Nano Lett.*, 2013, **13**, 4044-4052.
30. V. G. Dubrovskii, N. V. Sibirev, G. E. Cirlin, J. C. Harmand and V. M. Ustinov, *Phys. Rev. E*, 2006, **73**, 021603.

TOC